Int. J. Electrochem. Sci., 15**(2020)** 2973 – 2986, doi: 10.20964/2020.04.53

International Journal of ELECTROCHEMICAL SCIENCE
www.electrochemsci.org

Effect of CO_3^{2-} on the Electrochemical Behaviour of 14Cr12Ni3Mo2VN Stainless Steel in a Sodium Chloride Solution

Quan-de Li [1,2,3],Dou Ran[1],Fu-qiang Zhai[4],Wei-hua Guo[2,3],Xiu-fang Gong[2,3],Rong Ni[2,3], Ying Jiang[2,3],Xian-long Gong[2,3],Jun Dai[2,3],Hui-min Meng[1,],Bin Long[2,3,*]*

[1]Institute of Advance Materials and Technology, University of Science and Technology Beijing, Beijin g 100083, China
[2] State Key Laboratory of Long-life High Temperature Materials ,Deyang 618000, China
[3] Dongfang Turbine Co.,LTD, Deyang 618000, China
[4] Research Institute for New Materials Technology, Chongqing University of Arts and Sciences, Yongchuan Chongqing 402160, China;
[*]E-mail: menghm16@126.com, longb@dongfang.com

Received: 6 December 2019/ *Accepted:* 11 February 2020 / *Published:* 10 March 2020

The corrosion behaviour of 14Cr12Ni3Mo2VN martensitic stainless steel in a chloride solution with 20 mmol·L^{-1} Na_2CO_3 was investigated using X-ray photoelectron spectroscopy, open circuit potential analysis, electrochemical impedance spectroscopy, potentiodynamic polarization analysis, Mott-Schottkyanalysis,scanning electron microscopy and energy dispersive spectroscopy.It was found that the passivation films that form on14Cr12Ni3Mo2VN stainless steel in different test solutions were mainly composed of oxides and hydroxides of Fe, Cr and Mo. The formation and content of Cr_2O_3 in the passivation film were promoted and increased by the addition of CO_3^{2-} in solution, but the hydroxylation of Fe in the passivation film also occurred. The addition of CO_3^{2-} reduced the self-corrosion potential of 14Cr12Ni3Mo2VN and the donor density N_d of the passivation film, inhibited the number and activation of metastable pits on the electrode surface, improved the pitting potential and impedance of the passivation film, and increased the corrosion resistance of the material. Fe, Cr,V and Mo in the corrosion pit were selectively dissolved, demonstrating that Fe migrated to the solution in the form of ions, while Cr,V and Mo deposited in the pit in the form of oxides or hydroxides. CO_3^{2-} had no significant effect on the selective dissolution and migration of alloying elements in the matrix but it could significantly reduce the repassivation potential and increase the difficulty of repassivation in the activated pits.

Keywords: Stainless steel;Blade; Passivation;Electrochemistry;Corrosion

1. INTRODUCTION

Blades are the most important part of steam turbines because they convert the flowing energy of steam into useful work[1]. Blade failure often leads to plant failure and increases maintenance time

and cost[2-4]. In serious cases, the whole stage impeller and even the whole turbine can be damaged by blade failure. To increase the safety of the steam turbine and prevent the corrosion of the last stage turbine blade and to reduce the influence of blade failure on the safe operation of the steam turbine[5-7], the concentration of impurities in the feed water is strictly controlled[8].

However,in the Wilson zone of the low-pressure cylinder (the dry and wet steam transfer area), the steam begins to condense into liquid water, and the impurities in the steam that enter the turbine flow system during shutdown or operation of the turbine (such as Cl^- and CO_2) are redistributed[9,10]. By changing the water composition, part of the passivation film on the blade surface is destroyed and exposed to the active substrate, resulting in the formation of a corrosion battery with the passivation surface and promoting the development of pits on the blades that work in the Wilson zone[11,12].

At present,finite elemental tools and a fracture mechanics theory have been used to research the life of steam turbine blades and to estimate the residual life of blades that have been operating for many years.At the same time, the study of blade corrosion is mainly based on the corrosion or fracture of the blade to predict the corrosion affecting factors and the corrosion process[6,11].However, few studies have reported on the influence of CO_3^{2-}, which is produced by the reaction of carbon dioxide entering the condensed water with an alkaline substance that was added to the condensed water[13,14], on the corrosion behaviour of turbine blades[15,16].

Therefore, it is necessary for the safe operation of steam turbines to study the influence of CO_3^{2-} on blade corrosion.Herein, the exact corrosion behaviour and process of 14Cr12Ni3Mo2VN martensitic stainless steel is investigated, and the related corrosion mechanism is discussed.The experimental results can provide a theoretical basis and data support for practical steam turbine operation and choosing appropriate blade materials.

2. EXPERIMENTAL

2.1 Working electrode preparation

14Cr12Ni3Mo2VN martensitic stainless steel specimens were used, and their chemical composition is shown in Table 1.

Table 1. Chemical composition of 14Cr12Ni3Mo2VN stainless steel

Alloy	C	Si	Mn	S	P	Cr	Ni	Mo	V	N	Fe
% wt	0.15	0.12	0.75	0.073	0.013	11.50	2.97	1.61	0.28	0.034	balance

2.2 Experimental

The samples (10 mm×10 mm×10 mm) were cold mounted with an epoxy resin to prevent crevice corrosion, and a 1 cm^2 exposed area was used as a working electrode. Before the experiment, the working electrode was polished step by step to a mirror-likefinish with a grinding machine, washed

in distilled water and eventually dried by hot air just before being introduced into the electrochemical setup.

The tests were performed with a conventional three-electrode setup. A platinum plate was used as a counter electrode, and an SCE (saturated calomel electrode) was used as a reference electrode.The experimental electrochemical media were an NaCl solution (50 mmol·L^{-1}) and an NaCl(50 mmol·L^{-1})+ Na_2CO_3(20 mmol·L^{-1}) solution. Before the electrochemical tests, the working electrode was immersed in an NaCl solution purged with 99.999% argon for 72h.

Before testing, the open circuit potential (OCP vs. SCE) was obtained after running for 5 min and then stabilizing. The scan rate was set to 1 mV·s^{-1}, and the scanning range started from -800 mV(vs. SCE) and progressed to an anodic potential value. When the anodic polarization current density reached 1 mA·cm^{-2}, a reverse scan was immediately carried out until it intersected with the anodic polarization curve, and then the test was stopped. Electrochemical impedance spectroscopy (EIS) was carried out in a frequency range of 10^5-10^{-2} Hz with an amplitude of 10 mV. ZSimpWin software was used for data fitting analysis.A Mott-Schottky measurement was taken between -0.2 and 1.0 V (vs. SCE) with an ac signal amplitude of 10 mV. The test frequency was 1 kHz, and each parallel sample was tested at least 3 times for all of the above measurements.

X-ray photoelectron spectroscopy (XPS) elemental analysis was performed on the passivated film that formed on the surface of the sample immersed in the argon-purged solution for 72 h. Fe 2p,Cr 2p,Ni 2p and Mo 3d maps were tested by a monochromatic Al Kα light source (hυ=1486.6 eV). XPS analysis was tested to a depth of approximately 5 nm. XPS PEAK41 software was used for data analysis.The Shirley-type background was first subtracted, and then the peaks of each spectrum were segmented according to the binding energy that corresponded to the oxidation state of the matter in that phase.

After testing, the samples were rinsed with ethanol and deionized water and dried with cold air. The corrosion micromorphology of the working electrode surface was observed by scanning electron microscopy (SEM), and the composition was measured by energy dispersive spectroscopy(EDS).

3. RESULTS AND DISCUSSION

3.1. Xps test

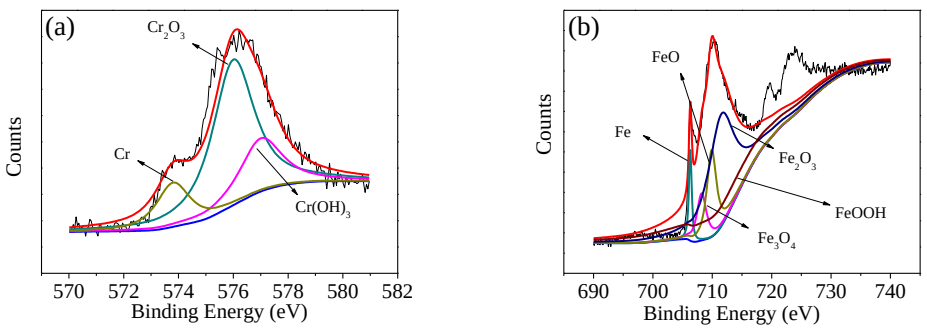

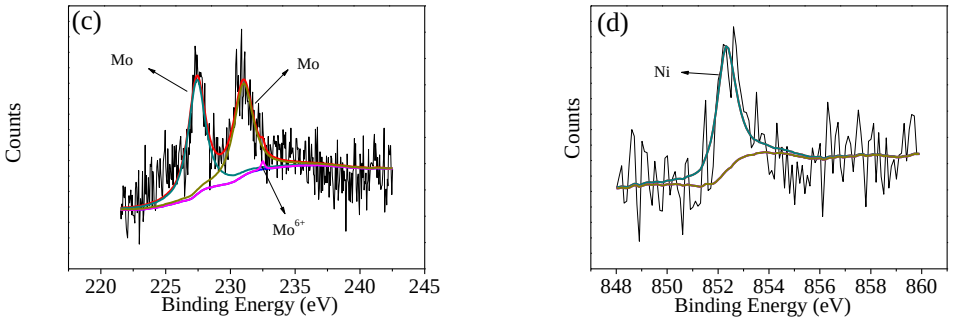

Figure 1. XPS curves of the 14Cr12Ni3Mo2VN samples in solutions with 50 mmol·L^{-1}NaCl for 72h:(a)Cr, (b)Fe, (c)Mo, and (d)Ni.

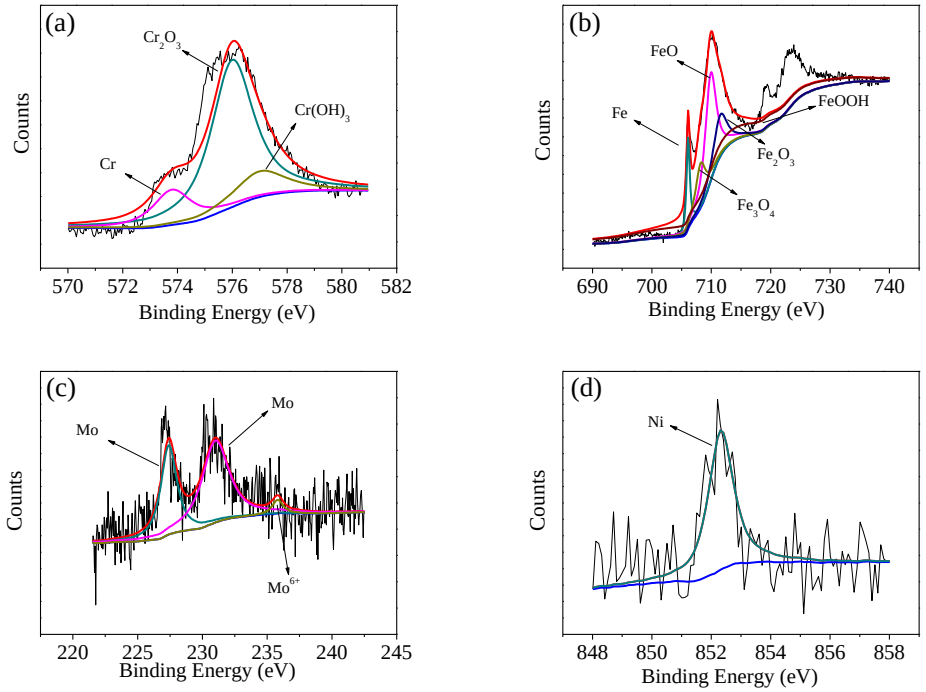

Figure 2. XPS curves of the 14Cr12Ni3Mo2VN samples in solutions with 50 mmol·L^{-1}NaCl +20 mmol·L^{-1} Na_2CO_3 for 72h:(a)Cr,(b)Fe,(c)Mo, and(d)Ni.

The spectra of Fe 2p, Cr 2p, Ni 2p and Mo 3d for the passivation films generated in different solutions are shown in Fig. 2 and Fig. 3.The NIST atomic spectrogram database and references[17-25]are used as the primary basis for elemental fitting, and the binding energy of the elemental oxidation states is shown in Table 2.The passivation films in the two solutions are mainly composed of oxides and hydroxides of Fe, Cr and Mo. Other studies have also shown that most passivation films on the surface of stainless steel are mainly composed of Cr_2O_3 in the inner layer and Fe_3O_4 in the outer layer.Cr is considered to be the most important element in stainless steel passivation films because Cr oxides can protect the stainless steel matrix[17,19,23].

Cr mainly exists in the form of Cr_2O_3/576.0 eV and $Cr(OH)_3$/577.0 eV(Fig. 1a and in Fig. 2a). The content of Cr_2O_3 in the passivation film increases from 61.77% to 69.45%, while the content of $Cr(OH)_3$ decreases from 22.87% to 14.91% with the appearance of CO_3^{2-} in the solution; the above results may be due to the increase of OH^- caused by the hydrolysis of CO_3^{2-} in the solution, which promotes the formation of the more stable Cr_2O_3[18].Fe mainly forms the following oxides: FeO, Fe_2O_3, Fe_3O_4 and FeOOH. It is generally believed that the peaks of FeO and Fe_3O_4 are very close, and it is difficult to determine the oxide composition of iron in the passivation film by analysing the valence state. However, FeO is an unstable oxide, so it is generally believed that Fe^{2+} exists because Fe_3O_4 is generated in the passivation film[22].The content of FeOOH in the passivation film increases from 31.94% (Fig. 1b) to 45.60% (Fig. 2b) with the addition of CO_3^{2-} in the solution; that is, Fe in the passivation film shows obvious hydroxylation.The XPS spectra of Mo in the passivation films formed on14Cr12Ni3Mo2VN stainless steel in different solutions are shown in Fig.1c and Fig.2c.

Because the Mo $3d_{5/2}$ and Mo $3d_{3/2}$ spin orbitals are coupled, the Mo spectra show bimodal peaks. Analysis of the passivation film shows that Mo oxides in the passivation film mainly exist in stable Mo^{+6} but not in unstable Mo^{+4}.In Fig. 1d and Fig. 2d, Ni/852.3 eVis observed in the passivation films formed in both solutions, which showed that the Ni in the passivation film is metallic and is in good agreement with other research conclusions[23-25].

Table 2. Binding energy of oxidation states of each element

Element	Peak	Binding energy
Fe	$2p_{3/2}$	Fe/706.5eV； FeO/709.9eV； Fe_3O_4/708.2eV； Fe_2O_3/711.5eV； FeOOH/712eV
Cr	$2p_{3/2}$	Cr /573.8 eV； Cr_2O_3 /576.0 eV； $Cr(OH)_3$/577.0 eV； CrO_3 /573.8 eV；
Ni	$2p_{3/2}$	Ni /852.32 eV； NiO/854 eV； $Ni(OH)_2$/855.78 eV
Mo	$3d_{5/2}$	Mo /227.4 eV； Mo^{4+} /228.8 eV； Mo^{6+} /232.5 eV；
	$3d_{3/2}$	Mo /231 eV； Mo^{4+} /234.2 eV； Mo^{6+} /235.8 eV；

3.2 Open circuit potentials

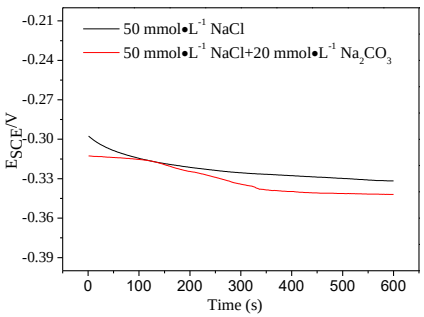

Figure 3. Open circuit potentials for the 14Cr12Ni3Mo2VN martensitic stainless steel samples in solutions with different concentrations of CO_3^{2-}.

The open circuit potentials (OCPs) of the 14Cr12Ni3Mo2VN samples in NaCl solutions with different concentrations of CO_3^{2-} are depicted in Fig. 3.The open circuit potential of 14Cr12Ni3Mo2VN stainless steel shifts from -0.332 V to -0.342V with increasing CO_3^{2-} concentration, which may be caused by CO_3^{2-} hydrolysing OH^- in solution (Equations (1) and (2)). Cl^- in solution undergoes competitive adsorption on the electrode surface, resulting in more OH^- adsorption on the electrode surface[26];the above significantly hydroxylates Fe in the passivation film and reduces the stable open circuit potential of the working electrode.

$CO_3^{2-} + H_2O = HCO_3^- + OH^-$ (1)

$HCO_3^- + H_2O = H_2CO_3 + OH^-$ (2)

3.3 Potentiodynamic polarization

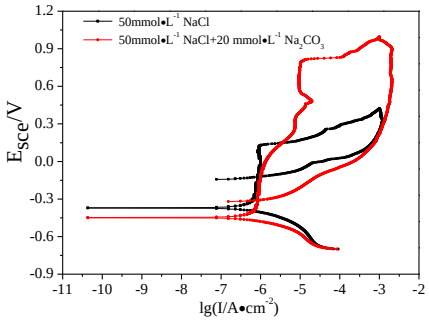

Figure 4. Potentiodynamic polarization curves of the 14Cr12Ni3Mo2VN martensitic stainless steel samples in solutions with different concentrations of CO_3^{2-}.

The potentiodynamic polarization curves of the 14Cr12Ni3Mo2VN samples in solutions with different concentrations of CO_3^{2-} are shown in Fig. 2.The potential value corresponding to the current density rapidly increasing to 100 $\mu A \cdot cm^{-2}$ on the polarization curve was the pitting potential(E_{pit}). The potential at the intersection of the polarization curve and the anodic polarization curve was the protection potential(E_{rp}).All curves of the cathodic polarization slope in Fig. 4 are very close, indicating that there is no obvious effect with the addition of CO_3^{2-} on the cathodic polarization rate of 14Cr12Ni3Mo2VN stainless steel.The addition of CO_3^{2-} mainly affects the anodic process[27].

The corrosion current (I_{corr}) of the working electrode does not change significantly and remainsat approximately 220 nA. However, the corrosion potential(E_{corr}) decreases from -0.371 V to -0.449V, the E_{pit} increases from 0.290 V to 0.831V, and the intersection of $E_{rp}$with the anode decreases from -0.124 V to -0.312 V due to the addition of CO_3^{2-}.This may be caused by the competitive adsorption of OH^- from CO_3^{2-} hydrolysis (Equations(1) and (2)) and Cl^- on the electrode surface, which changes from being dominated by Cl^- to being dominated by OH^-; the above results in the formation of a more protective Cr_2O_3 passivation film on the working electrode surface[28-30].An obvious current peak (approximately 20 μA) appears in the electrodynamic polarization curve at 0.482V(vs. SCE).After the peak appears, the current does not increase to the E_{pit} with increasing

potential but disappears with increasing scanning potential, which may be caused by the electrochemical reaction of Cr_2O_3 in the passivation film being oxidized to CrO_4^{2-}.

A hysteresis ring and peak current density appear in the dynamic potential polarization curves during the reverse scan at different concentrations. For the reverse scan of potential, the current density does not immediately decrease, as there is a section where it increases before starting to decrease.This is because the passivated film on the surface of the 14Cr12Ni3Mo2VN stainless steel electrode is broken down during the forward scan,which leads to pitting corrosion occurring on the surface of the electrode[31].A blocking area isformed due to the accumulation of corrosion products in the anodic corrosion pit, resulting in an increase in the concentration of metal cations in the occlusion area. To maintain electrical neutrality in the corrosion pit, Cl^- moves from the outside of the corrosion pit and continuously migrates and accumulates inside of the corrosion pit. As a result, the concentration of Cl^- in the hole constantly increases.Due to the high conductivity of the concentrated salt solution in the corrosion area, the internal resistance of the occluded battery is very low, and corrosion is ongoing[32,33].At the same time, the solubility of oxygen is very low, and diffusion is difficult, leading to the development of pitting corrosion and hindering the repair of the metal passivation film.Even the reverse scanin the negative potential direction can not immediately prevent the further expansion of pitting corrosion, thus resulting in a continuous increase in current density[34].

However, each reverse scan curve intersects the forward scan curve at a certain potential, and then the current density remains lower than that of the forward scan, indicating that a protective passivation film can be formed on the surface of each sample at this time.Unfortunately, with increasing concentrations of CO_3^{2-}, the E_{rp} decreases, as shown in Fig. 4, indicating the increasing difficulty of repairing the corroded passivation film.

3.4 Electrochemical impedance spectroscopy

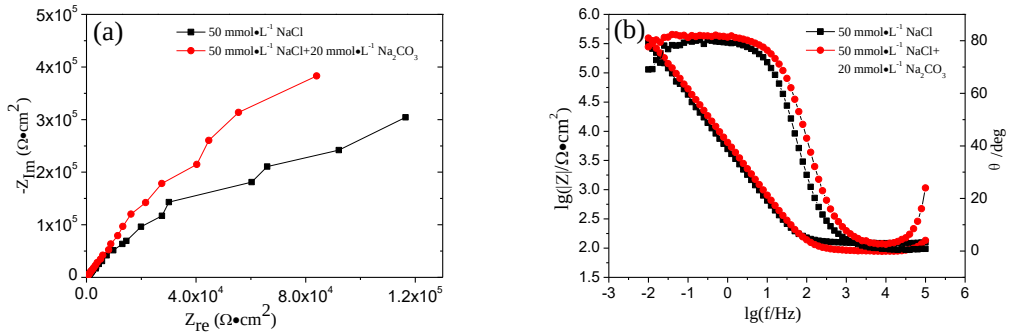

Figure 5. Electrochemical impedance spectroscopy of 14Cr12Ni3Mo2VN in solutions with different concentrations of CO_3^{2-}:(a)Nyquistand (b)Bode plots.

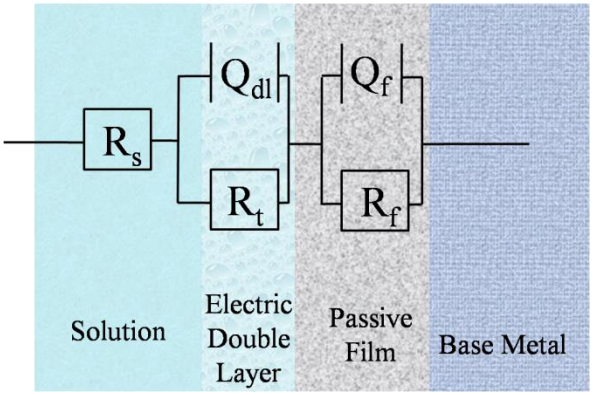

Figure 6. Equivalent circuit model from electrochemical impedance spectroscopy.

The electrochemical impedance spectroscopy test results for 14Cr12Ni3Mo2VN stainless steel indifferent concentrations of CO_3^{2-} solution can be seen (see Fig.5). The system impedance increases with the addition of CO_3^{2-}, indicating that the protection of the passivation film on the surface of 14Cr12Ni3Mo2VN stainless steel becomes better, the corrosion rate decreases, and the corrosion resistance is enhanced[35].

The electrochemical impedance spectroscopy in different solutions was analysed by the equivalent circuit shown in Fig. 6(see Table 3)[36],where R_s is the solution resistance, CPE(Q_f) is the passivation film capacitance, R_f is the passivation film resistance, CPE(Q_{dl}) and R_t are the capacitance and charge transfer resistance of the surface double layer, respectively, and CPE(Q) is generally used for the in-uniform distribution of the stainless steel surface current and high surface roughness.The CPE impedance value can be calculated by the following formula:

$$Z_Q = (j\omega)^{-n}/Y_0 \qquad (3)$$

where Y_0 is the admittance modulus of CPE, ω is the angular frequency, and n is the diffusion exponent of the CPE. Its value range is set to $0 \le n \le 1$. When n=0.5, the CPE is considered a Warburg impedance.When n=1, the CPE is considered to be anideal capacitor, and when $0.5 < n < 1$, the CPE is in a middle state between the above mentioned states.

Table 3. Parameters of the equivalent circuit

Solution	R_s/ ($\Omega \cdot cm^2$)	Q_{dl}		R_t/($\Omega \cdot cm^2$)	Q_f		R_f/ ($\Omega \cdot cm^2$)
		$Y_0/(\Omega^{-1} \cdot cm^{-2} \cdot S^{n1})$	n_1		$Y_0/(\Omega^{-1} \cdot cm^{-2} \cdot S^{n2})$	n_2	
50 mmol·L^{-1}NaCl	122.6	3.36×10^{-4}	0.86	735	3.81×10^{-5}	0.94	1.06×10^{6}
50 mmol·L^{-1} NaCl+20 mmol·L^{-1} Na_2CO_3	86.47	9.54×10^{-5}	0.91	945	2.92×10^{-5}	0.91	6.02×10^{6}

As shown in Table 3, the R_f of 14Cr12Ni3Mo2VN stainless steel is $1.06\times10^6 \Omega \cdot cm^2$ and rises to $6.02\times10^6 \Omega \cdot cm^2$ with the addition of CO_3^{2-}. With the addition of CO_3^{2-}, the impedance of the passivation film becomes larger, and the protection becomes better. This is mainly caused by the increase in the content of Cr_2O_3, which is better protectorin the passivation film.In addition, CO_3^{2-} may react with Fe or Cr on the surface of stainless steel to form $FeCO_3$ or $CrCO_3$ protective salt films with relatively low solubility[37,38].The corrosion resistance of the material fitted by the equivalent circuit

is in good agreement with the test results from the open circuit potential analysis, XPS and dynamic potential polarization analysis.

3.5. Mott-Schottky

According to the point defect model of a passivation film, a passivation film on the surface of stainless steel is an oxide film with a high density of doped point defectsand semiconductor characteristics.The passivation film formed on the surface of a metal or alloy usually has semiconductor properties[39,40]. When the passivation film contacts the solution, a space charge layer will be formed on the side of the passivation film, and a Helmholtz layer will be formed on the side of the solution.At this time, the solution and the semiconductor film carry opposite charges, and the excess charge of the semiconductor film will be distributed in a space charge layer.When the space charge layer is in a depleted state, the capacitance of the space charge layer and the measured electrode potential can be described and analysed by the Mott-Schottky equation[41].Different anions will be competitively adsorbed on the surface of stainless steel in the solutionand increasing the presence of CO_3^{2-} in the solution will reduce the adsorption of Cl^- on the surface of the stainless steel electrode; therefore, the above affects the corrosion characteristics of the material.

The space charge capacitance has the following relationship with the measured potential:

$$\frac{1}{C^2} = \frac{2}{\varepsilon\varepsilon_0 e N_d A^2}\left(E - E_{fb} - \frac{kT}{e}\right) \quad (4)$$

$$\frac{1}{C^2} = -\frac{2}{\varepsilon\varepsilon_0 e N_a A^2}\left(E - E_{fb} - \frac{kT}{e}\right) \quad (5)$$

$$W = \left[\frac{2\varepsilon\varepsilon_0}{eN_d}\left(E - E_{fb} - \frac{kT}{e}\right)\right]^{\frac{1}{2}} \quad (6)$$

where C is the space charge layer capacitance of the passivation film, F; E is the scanning potential, V; E_{fb} is the flat band potential, V; ε_0 is the vacuum dielectric constant, 8.85×10^{-14} F·cm^{-1}; ε is the relative dielectric constant at 15.6; N_D and N_A represent the donor and acceptor densities for n-type and p-type semiconductors, respectively, cm^{-3}; A is the sample area, which is set at1 in this paper, cm^2; K is the Boltzmann constant, 1.38×10^{-23}J·K^{-1}; e is the electron charge, 1.6×10^{-19}C; T shows the thermo dynamic temperature, K; and W is the thickness of the passivation film, 10^{-10} m. Equation (4) represents n-type semiconductor characteristics of a passivation film, while Equation (5) shows that of a p-type. Equation (6) represents the film thickness.

Fig. 7 shows the Mott-Schottky curve of the stainless steel samples in different concentrations of CO_3^{2-} solutions. It can be seen that the Mott-Schottky curve has roughly the same variation trend with 2 intervals. The slope of the fitted straight line is positive, showing an n-type semiconductor. The second interval,in which the slope is negative, demonstrates a p-type semiconductor. The main density of N_d is one of the important parameters to describe the passivation properties of the stainless steel samples. Table 4 shows the N_d values calculated by fitting the Mott-Schottky curve (Equation (4)).

With increasing CO_3^{2-}, the main density N_d of the passivation film donor decreases from 1.07×10^{21}cm^{-3} to 0.81×10^{21} cm^{-3}, which indicates that the point defects and transmission channels of the corrosion medium in the passivation film both decrease with the addition of CO_3^{2-}. Moreover, the charge transfer resistance and the difficulty of charge transfer both increase, and the electrode reaction

is relatively more difficult[42,43]. The experimental results are in good agreement with the XPS results.

According to Equation (6), when N_d decreases, the thickness of the passivation film W increases, and the stability of the passivation film becomes better, which shows that its corrosion resistance increases. The above indicates that with the addition of CO_3^{2-},the adsorption of Cl^- at the active point on the electrode surface isreduced; thus, the occurrence of pitting is inhibited.Cr tends to exist in the form of Cr_2O_3 in a passivation film formed in a weakly alkaline solution because of the hydrolysis of CO_3^{2-}, which increases the corrosion resistance of the material.According to the above results, the addition of CO_3^{2-} in solution can promote the reduction of the point defect density of the passivated film[44], increase the stability of the passivated film and slow down the occurrence of corrosion, which is in good agreement with the electrochemical impedance spectroscopy results.

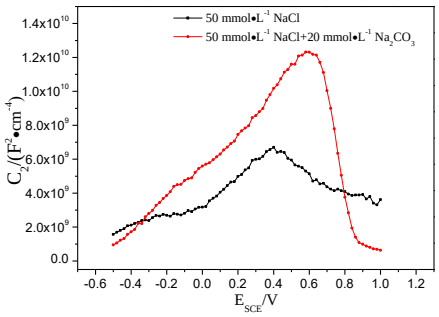

Figure 7. Mott-Schottky curves of the 14Cr12Ni3Mo2VN samples in solutions with different concentrations of CO_3^{2-}

Table 4. Donor density

Solution	$N_d/(10^{21}\ cm^{-3})$
50 mmol·L^{-1}NaCl	1.07
50 mmol·L^{-1} NaCl+20 mmol·L^{-1} Na_2CO_3	0.81

3.6. Morphology and composition analysis

SEM and EDS analyses were conducted on the samples after electropolarization, and the results of the pit morphologies on the surface of each sample are shown in Fig. 8. The 14Cr12Ni3Mo2VN stainless steel surface produces a large number of pits with a diameter of approximately 80 μm and a transverse to longitudinal ratio of approximately 1 (Fig.8a) in the solution without CO_3^{2-}. Only one pit is formed on the surface of the working electrode, with deep ends and a shallow centre,in the CO_3^{2-} added solution (Fig. 8b).The single pit may have formed due to the number of metastable active pitting spots generated during the electro dynamic scanning process being reduced by the improved corrosion resistance of the surface passivation film; furthermore,the current resulting from the potential scanning is concentrated in the pit, which resultsin rapid growth, connection and eventual formation of the large pit in Fig. 8b. At the same time, metastable pitting is inhibited in other parts of the electrode surface, and no other pits are formed.

Typical corrosion pits on the surfaces of the samples were selected for an EDS analysis of typical elements, and the results are shown in Fig. 9 and Fig. 10.According to the EDS analysis, the corrosion products of stainless steel are mainly composed of Fe, Cr, V and Mo.The products in the corrosion pit are mainly composed of Cr, V and Mo, and the relative contents of Cr, V and Mo in the corrosion pit are significantly higher than those in the stainless steel matrix, but the content of Fe in the corrosion pit is lower than that in the matrix[45].This indicates that after the selective dissolution of Fe, Cr, V, and Mo occurs,a pit is formed on the surface of the stainless steel electrode and extendsto the interior. Fe quickly migrates from the corrosion pit, while the migration rate of Cr, V and Mo is slow and deposition occurs to some extent, which leads to the relative increase of Cr, V and Mo in the corrosion pit[46-48].In addition, the oxygen content in the sample corrosion pit is significantly higher than that in the substrate, indicating that Cr, V and Mo may be deposited in the corrosion pit as oxides or hydroxides in the corrosion products[49,50].

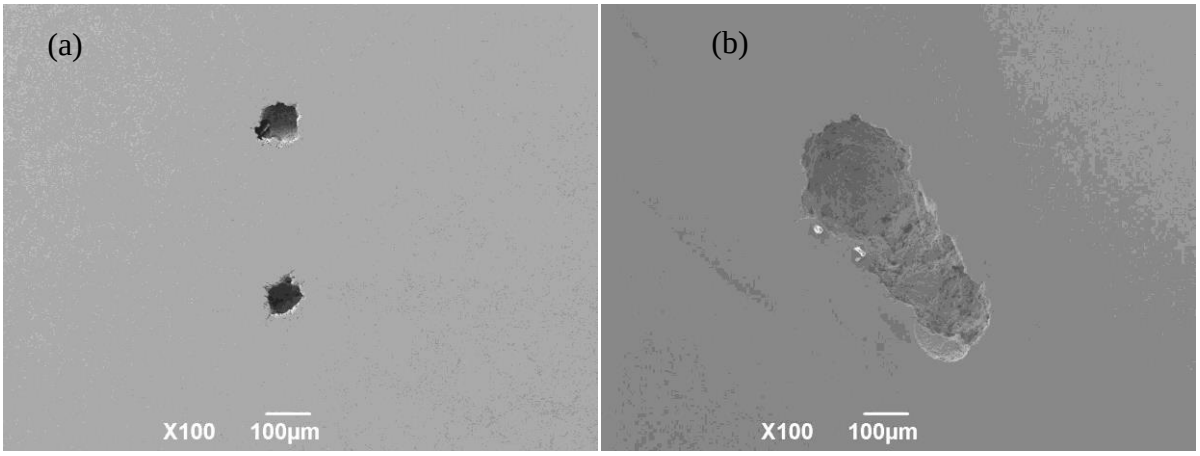

Figure 8. Pit morphologies of the 14Cr12Ni3Mo2VN martensitic stainless steel samples in solutions with different concentrations of CO_3^{2-}:(a)50 mmol·L^{-1}NaCland (b)50 mmol·L^{-1}NaCl +20 mmol·L^{-1} Na_2CO_3.

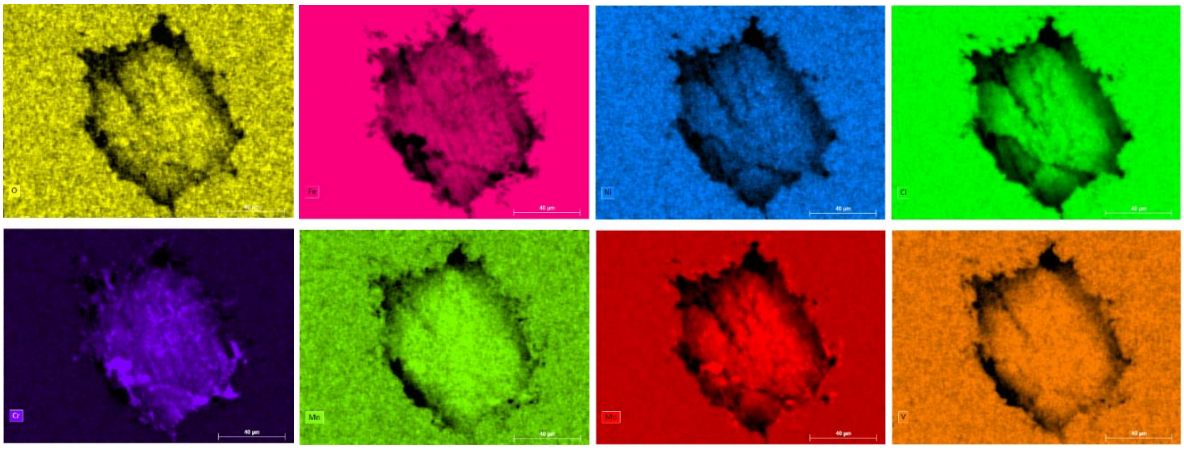

Figure 9.EDS of the pits in the 14Cr12Ni3Mo2VN martensitic stainless steel samples in the solution without CO_3^{2-}.

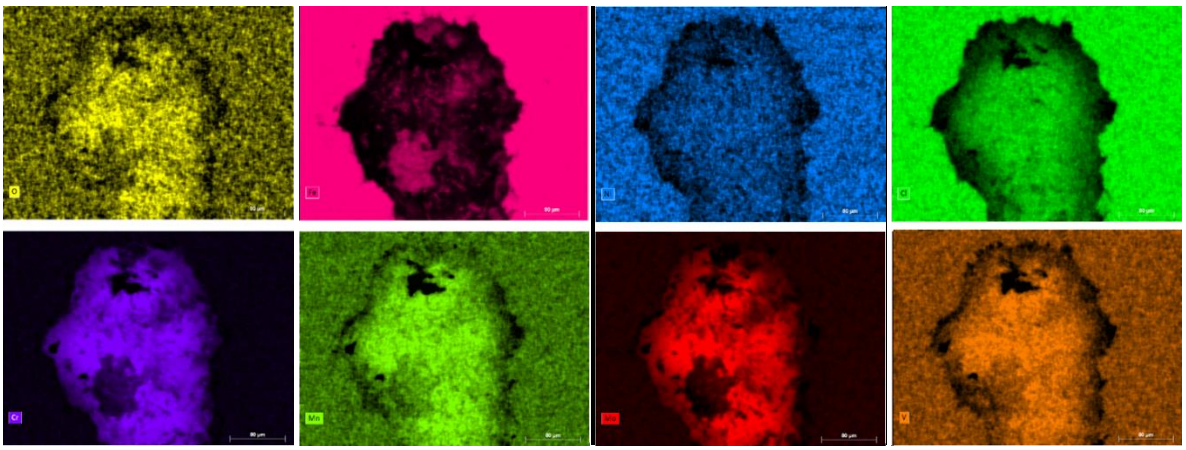

Figure 10.EDS of the pits in the 14Cr12Ni3Mo2VN martensitic stainless steel samples in the solution with CO_3^{2-}.

4. CONCLUSIONS

A passivation film of 14Cr12Ni3Mo2VN stainless steel in solution is mainly composed of oxides and hydroxides of Fe, Cr and Mo. CO_3^{2-} will promote the formation of Cr_2O_3 in the passivation film and the hydroxylation of Fe in the passivation film.

CO_3^{2-} will reduce the self-corrosion potential of 14Cr12Ni3Mo2VN; improve the pitting potential and impedance of the passivation film; reduce the donor density N_d of the passivation film; inhibit the number of point defects, metastable pits and activation points in the passivation film; increase the corrosion resistance of the material; and reduce the corrosion rate.

When stable pit corrosion of 14Cr12Ni3Mo2VN occurs, Fe migrates to the solution in the form of ions, while Cr, V and Mo aredeposited in the corrosion pit in the form of oxides or hydroxides. Thus, CO_3^{2-} has no significant effect on the selective dissolution and migration of elements but increases the difficulty of repassivation.

ACKNOWLEDGEMENTS
This work is financially supported by the fund of the State Key Laboratory of Long-life High Temperature Materials(No. DTCC28EE190230) and Sichuan Applied Foundation Projiect(No. 2019YJ0699).

References

1. Sławomir Dykas, Mirosław Majkut, Krystian Smołka, Michał Strozik,*Int. J. Heat.Mass Tran.,* 120 (2018) 9.
2. C.R.F. Azevedo, A. Sinátora, *Eng. Fai. Anal.,*16 (2009) 2290.
3. D.G. Hattingh, M.N. James, M. Newby, R. Scheepers, P. Doubell, *Theor.Appl.Fract.Mec.,*83 (2016) 125.
4. Jolanta Baran, *Energ,Convers, Manage.,*116 (2016) 18.
5. A. Ahmadpour, S.M.A. Noori Rahim Abadi, J.P. Meyer, *Energy,* 119 (2017) 675.

6. Sanjeev Saxena, J.P. Pandey, Ranjit Singh Solanki, Gaurav K. Gupta, O.P. Modi, *Eng. Fai. Anal.*,52 (2015) 35.
7. S. Cano, J.A. Rodriguez, J.M. Rodriguez, J.C. Garcia, F.Z. Sierra, S.R. Casolco,M. Herrera, *Eng. Fai. Anal.*, 97 (2019) 579.
8. J.A. Rodríguez, L. Castro, A.L. Tejeda, J.C. García, J.M. Rodríguez, E. Galindo,Y. El Hamzaouic, *Eng. Fai. Anal.*, 104 (2019) 39.
9. Marko Katinić, Dražan Kozak, Ivan Gelo, Darko Damjanović, *Eng. Fai. Anal.*, 106 (2019) 104136
10. Xu Han, Wei Zeng, Zhonghe Han, *Appl.Therm.Eng.*,164 (2020) 114538.
11. M. Nurbanasari, Abdurrachim, *Case. Stud.Eng. Fail. Anal.*,2 (2014) 54.
12. Ernst Plesiutschnig, Patrick Fritzl, Norbert Enzinger, Christof Sommitsch, *Case. Stud.Eng. Fail. Anal.*, 5–6 (2016) 39.
13. Akash Shukla, S.P. Harsha, *Mater.Today.*, 2(2015) 2056.
14. Loveleen Kumar Bhagi, Vikas Rastogi, Pardeep Gupta, Swastik Pradhan, *Mater.Today,* 5(2018) 28117.
15. Goutam Das, Sandip Ghosh Chowdhury, Ashok Kumar Ray,Swapan Kumar Das, Deepak Kumar Bhattacharya, *Eng. Fail. Anal.*, 10 (2003) 85.
16. A.P. Tschiptschin, C.R.F. Azevedo, *Eng. Fail. Anal.*, 12 (2005) 49.
17. V. Vignal, H. Krawiec, O. Heintz, D. Mainy, *Corros. Sci*.,1 67 (2013) 109-117.
18. Elise Gardin, Sandrine Zanna, Antoine Seyeux, Audrey Allion-Maurer, Philippe Marcus, *Corros. Sci.*, 167 (2018) 403-413.
19. Bijun Xie, Mingyue Sun, Bin Xu, Chunyang Wang, Haiyang Jiang, Dianzhong Li, Yiyi Li, *Corros. Sci.*, 147 (2019)41-52.
20. Dj. Mandrino, C. Donik, Vacuum, 86 (2011) 18-22.
21. Jian Wang, Yishi Cui, Jingang Bai, Nan Dong, Ying Liu, Caili Zhang, Peide Han, Mater. Lett., 252 (2019)60-63.
22. Zuocheng Wang, Antoine Seyeux, Sandrine Zanna, Vincent Maurice, Philippe Marcus, Electrochim. Acta, 329 (2020) 135159.
23. M. Kovendhan, Hari Kang, Sangmin Jeong, Jong-Sang Youn, Inhwan Oh, Young-Kwon Park,Ki-Joon Jeon, Environ Res,. 173 (2019) 549-555.
24. L.B. Coelho, S. Kossman, A. Mejias, X. Noirfalise, A. Montagne, A. Van Gorp,M. Poorteman, M.-G. Olivier, Surf, Coat,Tech,. 382 (2020) 125175.
25. Tigang Duan, Wenshan Peng, Kangkang Ding, Weimin Guo, Jian Hou, Wenhua Cheng, Shaotong Liu, Likun Xu, Ocean, Eng., 189 (2019) 106405.
26. C.J. Scheuer, F.A.A. Possoli, P.C. Borges, R.P. Cardoso, S.F. Brunatto, *Electrochim. Acta,* 317 (2019) 70.
27. J. Li, C.W. Du, Z.Y. Liu, X.G. Li, M. Liu, *Constr. Build. Mater.*, 189 (2018) 1286.
28. Xuanpeng Li, Yang Zhao, Wenlong Qi, Junfeng Xie, Jidong Wang, Bin Liu,Guanxin Zeng, Tao Zhang, Fuhui Wang, *Appl. Surf. Sci.*, 469 (2019) 146.
29. Hong Luo, Qiang Yu, Chaofang Dong, Gang Sha, Zhenbao Liu, Jianxiong Liang,Li Wang, Gang Han, Xiaogang Li, *Corros. Sci.*, 139 (2018) 185.
30. M.J.K. Lodhi, K.M. Deen, M.C. Greenlee-Wacker, Waseem Haider, *Addit. Manuf.*, 27 (2019) 8.
31. I.G. Ogunsanya, C.M. Hansson, *Materialia,* 6 (2019) 100321.
32. G. Tranchida, M. Clesi, F. Di Franco, F. Di Quarto, M. Santamaria, *Electrochim. Acta,* 273 (2018) 412.
33. J. Li, C.W. Du, Z.Y. Liu, X.G. Li, M. Liu, *Constr. Build. Mater.*, 189 (2018) 1286.
34. Xuanpeng Li, Yang Zhao, Wenlong Qi, Junfeng Xie, Jidong Wang, Bin Liu,Guanxin Zeng, Tao Zhang, Fuhui Wang, *Appl. Surf. Sci.*, 469 (2019) 146
35. Fenfen Yang, Huijun Kang, Enyu Guo, Rengeng Li, Zongning Chen, Yanhua Zeng,Tongmin Wang, *Corros. Sci.*, 139 (2018) 333.

36. Hong Luo, Qiang Yu, Chaofang Dong, Gang Sha, Zhenbao Liu, Jianxiong Liang,Li Wang, Gang Han, Xiaogang Li, *Corros. Sci.*, 139 (2018) 185.
37. Odhiambo John Gerald, Li WenGe, Li Zhang, Zhao YuanTao, Li Cheng Lon, *Mater. Chem. Phys.*, 239 (2020) 122010.
38. L. Pan, C.T. Kwok, K.H. Lo, *J. Mater. Process. Tech.*, 277 (2020) 116448.
39. J. Izquierdo, L. Martín-Ruíz, B.M. Fernández-Pérez, R. Rodríguez-Raposo, J.J. Santana,R.M. Souto, *Electroanal. Chem.*, 728 (2014) 148.
40. Zhenwei Yan, Xianjie Yuan, Zhaojun Tan, Mingqi Tang, Zaiqiang Feng, *Int. J. Electrochem. Sc.*,13(2018)353.
41. A. Fattah-alhosseini, S. Vafaeian, *J. Alloy. Compd.*, 639 (2015) 301.
42. Sabrina Marcelin, Benoit Ter-Ovanessian, Bernard Normand, *Electrochem. Commun.*, 66 (2016) 62.
43. M. BenSalah, R. Sabot, E. Triki, L. Dhouibi, Ph. Refait, M. Jeannin, *Corros. Sci.*, 86 (2014) 61.
44. L.V. Taveira, M.F. Montemor, M. Da Cunha Belo, M.G. Ferreira, L.F.P. Dick, *Corros. Sci.*, 52 (2010) 2813.
45. Miranda, Jesualdo Pereira Farias, Luciano Andrei Bergmann, Jorge F. dos Santos, *J. Mater. Res. Technol.*, 2019;8(2):1878.
46. Y.Y. Li, Z.Z. Wang, X.P. Guo, G.A. Zhang, *Corros. Sci.*, 147 (2019) 260.
47. Xiangfeng Zhang, Jun Wang, Hongyuan Fan, Dong Pan, *Appl. Surf. Sci.*, 440 (2018) 755.
48. Decheng Kong, Chaofang Dong, Xiaoqing Ni, Liang Zhang, Jizheng Yao,Cheng Man, Xuequn Cheng, Kui Xiao, Xiaogang Li, *J. Mater. Sci. Technol.*, 35 (2019) 1499.
49. Mirosław Szala, Karolina Beer-Lech, MariuszWalczak , *Eng. Fail. Anal.*, 77 (2017) 31.
50. Sicong Shen, Xiaolong Song, Qizhen Li, Xinfeng Li, Ruihua Zhu, Gongxian Yang, *Mat. Sci. Eng.A.*, 740-741 (2019) 243.